Defects in the twist-bend nematic phase: Stabilities and instabilities of focal conic domains and related topics

Maurice Kleman, Kanakapura S. Krishnamurthy

Defects in the twist-bend nematic phase: Stabilities and instabilities of focal conic domains and related topics

Maurice Kleman[*]

Institut de Physique du Globe de Paris, Université Sorbonne Paris Cité 1, rue Jussieu, 75238 Paris cedex 05, France

Kanakapura S. Krishnamurthy[†]

Centre for Nano and Soft Matter Sciences, P.O. Box 1329, Jalahalli, Bangalore 560013, India

This article provides an explanation for the instability of toric focal conic domains and the stability of parabolic focal conic domains in the twist-bend nematic (N_{TB}) phase, by reason of the presence (the first case) or absence (the second case) of defect densities attached to the conics, which are disclinations. This result is obtained after a reminder of the theory of attached defects (the extended Volterra process) and is followed by its usage in other cases (dislocations, disclinations, dispirations, double helices) in the N_{TB} phase. The notion of spin disclination is introduced.

I. INTRODUCTION

The twist-bend nematic (N_{TB}) phase has been actively studied in the past few years for its fundamentally significant, and often challenging, properties. The heliconical structure of the N_{TB} phase, with its associated spontaneous flexoelectric polarization, was first envisaged by Meyer [1]. Much later, its possible occurrence in nematogens of achiral molecules with negative bend elastic constant was foreseen by Dozov [2]. Indeed, the molecules in the N_{TB} phase assemble into chiral structures, left or right with equal probability and it is this chirality that is at the origin of its flexoelectric properties [3,4]. Optically, the N_{TB} phase reveals itself in spontaneously developed periodic patterns, not fully understood, such as brought out by Panov *et al.* [5], which have led to a more definitive identification of the phase with its nanometric pitch. See also Refs. [6–8] and the bibliography therein.

A most striking feature is the instability of toric focal conic domains (TFCDs, eccentricity $e = 0$) such as in Fig. 1, which nucleate in the homeotropic N_{TB} state derived electrically from the homeotropic N state. TFCDs are unstable and gradually transform into parabolic focal conic domains (PFCDs) or into double helices (DHs). A classic arrangement of resulting PFCDs [9] is illustrated in Fig. 2(b); the DHs are shown in Figs. 3(b)–3(d); see Ref. [10] for the TFCD instability at the $N \Rightarrow N_{TB}$ transition under an electric field.

PFCDs (eccentricity $e = 1$) occur easily in the N_{TB} phase under dilative strains [4]; they generally form sets of parallel parabolas which are stable [Fig. 2(a)] or as isolated defects. However, usual focal conic domains (FCDs, $0 < e < 1$) are most often observed as belonging to tilt boundaries, i.e., sets of parallel ellipses with equal eccentricities e. Double helices (DHs), first observed in layered media by Williams [11], are frequent; see Fig. 3.

A. Experimental methods

The optical textures of defect states of the N_{TB} phase presented in this paper are from our experimental studies on the dimeric mesogen 1",7"-bis(4-cyanobiphenyl-4'-yl)heptane (CB7CB) and its 1:1 (by weight) mixture with n-heptyloxy cyanobiphenyl (7OCB). CB7CB was synthesized by two of the authors (M.B.K. and C.V.Y.) [10]; the synthetic procedure followed is described in the Supplemental Material of Ref. [12]. The phase sequence of CB7CB determined from polarization microscopy was: isotropic (116°C) N (103°C) N_{TB}. The phase behavior of various mixtures of CB7CB and 7OCB is discussed in Ref. [12]. The particular mixture used here had the following transitional sequence: isotropic (82.0°C) N (35°C) N_{TB}. Optical textures were studied using a Carl-Zeiss Axio Imager.M1m polarizing microscope with an AxioCam MRc5 digital camera. The sample cells, designed for either planar or 90°-twisted nematic configuration, were supplied by M/s AWAT, Poland. Sample temperature, accurate to ±0.1°C, was maintained using an Instec HCS402 hot-stage connected to a STC200 temperature controller. In electric field experiments, the driving voltage was from a Stanford Research Systems function generator (DS345) coupled to a FLC Electronics voltage amplifier (model A800). The field frequency and rms voltage were measured with a Keithley-2002 multimeter.

B. Content

This article is devoted to a physical description of these characteristics on the theoretical basis of the extended Volterra process; see Ref. [13], where it is shown that the analysis of the shape, mobility, and relaxation properties of a disclination L in a liquid crystal can be expressed in terms of densities of continuous dislocations, disclinations, and dispirations attached to it, thus providing, can we say, a qualitative description of the stresses and strains. The previously mentioned textural features of the N_{TB}

————
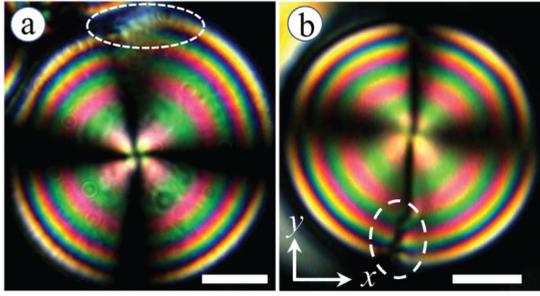[*]kleman@ipgp.fr
[†]murthyksk@cens.res.in

FIG. 1. Imperfect toric focal conic formations in the N_{TB} phase of a 20-μm-thick CB7CB layer in a 90°-twist cell. (a) 8.1 V, 10 kHz and (b) after switch off from 15 V, 1 kHz. Defect regions are encircled. The appearance of these defects is a first step in the transformation of TFCDs into PFCDs. Notice the small grainy defects all along circles. Crossed polarizers with their axes along (x, y). Scale bar: 10 μm.

phase constitute a set of most interesting observations of the role of these attached defects, in particular in the instability of TFCDs, the stability of PFCDs, their modifications under the action of stresses. We start by a reminder of the theory of attached defects.

II. THE THEORY OF ATTACHED DEFECTS

A. The Volterra process and the matching condition

The classic Volterra process [13] states that a line defect in an ordered material results from a thought experiment consisting of the following steps: (1) a relative rigid displacement $\mathbf{d}(\mathbf{M})$ of the lips Σ^+ and Σ^- of a cut surface Σ bordered by the line L, (2) the introduction of a piece of perfectly ordered material in the void thus created (or the removal of doubly covered material), (3) the elastic relaxation of the whole.

Being a rigid displacement, $\mathbf{d}(\mathbf{M})$ is the sum of a translation $\mathbf{b}$ and a rotation $\mathbf{f} \times \mathbf{OM}$:

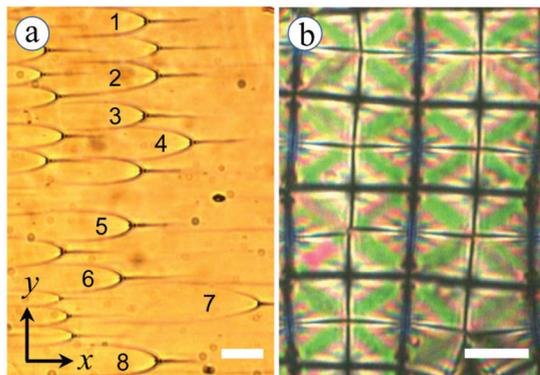$$\mathbf{d}(\mathbf{M}) = \mathbf{b} + \mathbf{f} \times \mathbf{OM},$$

FIG. 2. Focal conics in the N_{TB} phase of CB7CB, close to its setting point: (a) PFCDs and FCDs (see later for eccentricities of the numbered conics here), (b) electrically generated (8 V, 1 kHz) PFCDs, arranged along the substrate rubbing direction. The precursor N was: (a) aligned along x, (b) homeotropic. Single polarizer along x in (a), crossed polarizers along x and y in (b). Scale bar: 20 μm. Sample thickness = 20 μm.
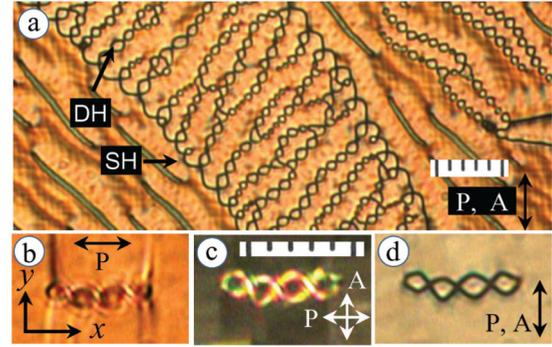

FIG. 3. (a) Single-helical (SH) and double-helical (DH) defects formed in the N_{TB} phase of the mixture of CB7CB and 7OCB (1:1 by weight) held in a 90°-twist cell at 31°C. The dark rails parallel to the DHs of the right upper part are bunches of screw dislocations of small Burgers vectors, whose total Burgers vector is probably of the same order as the giant Burgers vector of the DHs. The central diagonal region is oppositely twisted relative to outer regions. The disclinations separating the oppositely twisted regions in the precursor N phase develop into SH defects in the N_{TB} phase. The DHs run in the direction of midplane nematic director. The helices also form by coalescence of drifting TFCDs that evolve during the transition from electric homeotropic Freedericksz state to the planar state (b)–(d). Scale: 5 μm each small div. Double arrows represent polarizers. Sample thickness: (a) 5 μm, (b) 20 μm.

where $\mathbf{b}$ is the Burgers vector of the *dislocation* part of the displacement and $\mathbf{f} = 2 \sin \Omega/2 \, \boldsymbol{\varpi}$ (see Ref. [13] for the proof of this formula) the Frank vector of the *disclination* part (Ω is the angle of rotation, $\boldsymbol{\varpi}$ is a unit vector along the rotation axis, $\mathbf{O}$ being the origin along this axis). Observe that $|\Omega| = 2\pi$ disclinations cannot be represented by the expression $\mathbf{f} = 2 \sin \Omega/2 \, \boldsymbol{\varpi}$; in the Volterra process a $k = 1$ defect is the sum of two $k = 1/2$ defects in contact. The notation k stands for an angle of rotation $\Omega = 2\pi k$.

In order that the molecular structure of the added material matches perfectly to the lip molecular structure, $\mathbf{b}$ and $\mathbf{f} \times \mathbf{OM}$ have to be symmetry elements of the ordered material (*matching condition*). These are *perfect* dislocations (disclinations). If this condition is not achieved, a *stacking fault* which carries extra energy takes place along the cut surface in the relaxed material; one speaks of an *imperfect* dislocation (disclination).

The symmetry elements we have in mind can be quantized symmetry elements as well as continuous ones (as they exist in liquid crystals).

B. Continuous defects

The above considerations implicitly assume that the displacement $\mathbf{d}(\mathbf{M})$ is small and the relaxation linear outside the core of the line defect. This condition is easy to achieve if the displacement is restricted to a small translation; in most cases $\mathbf{b}$ is empirically equal to a very few lattice parameters.

This condition of a small displacement cannot be achieved in the case of a generic disclination, although straight wedge disclination lines are possible in liquid crystals because the axis of rotation is along the line L; the large displacements at a distance from L are viscously relaxed. If L is curved, the
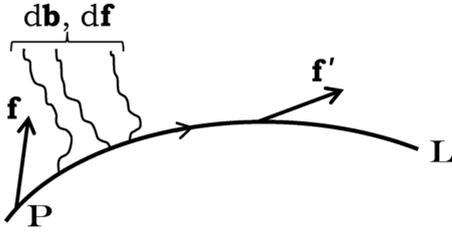
FIG. 4. Attached infinitesimal defects (dislocations, disclinations) along a disclination line L. The Frank vector **f** varies along the line in direction. **P** and **P**′ are close points.

rotation axis, which in the Volterra process is fixed in position, is no longer all over along the line. The solution is to let the Frank vector **f** vary along L, which requires the introduction of attached dislocations and disclinations. This is the *extended Volterra process* [13]. Consider indeed two close points **P** and **P**′ = **P** + **t**ds on the line (Fig. 4). The displacement of a point **M** ∈ Σ, seen from **P**, is $\mathbf{d_P}(\mathbf{M}) = \mathbf{f} \times \mathbf{PM}$; seen from **P**′ it is $\mathbf{d_{P'}}(\mathbf{M}) = \mathbf{f'} \times \mathbf{P'M}$. These two displacements are obviously not equal; the difference

$$\mathbf{d_{P'}}(\mathbf{M}) - \mathbf{d_P}(\mathbf{M}) = -\mathbf{f} \times \mathbf{t}ds + d\mathbf{f} \times \mathbf{PM} \qquad (1)$$

is the sum of a dislocation (the Burgers vector $d\mathbf{b} = -\mathbf{f} \times \mathbf{t}ds$ does not depend on **M**) and a disclination of Frank vector $d\mathbf{f}$, both attached to L between **P** and **P**′.

By the same reason as above, viz. the preference for a perfect matching, one expects that $d\mathbf{b}$ and $d\mathbf{f}$ are symmetry elements of the material, in so far as such symmetries exist. In crystalline solids, continuous symmetries do not exist and this *relaxation process* of the stresses around a disclination is absent. This is not so in liquid crystals. Continuous defects are prominent in the relaxation of quantized defects in nematics N and cholesterics N*, see [14]. They have the property to disperse away while remaining attached to the main line L, which is the process by which they relax the stresses carried by the line. Thus, they are not visible. But they provide a qualitative description of these stresses. If continuous defects play a role in the relaxation properties of the quantized defects, they also place limits on the relaxation processes since they are restricted somehow by the matching condition.

C. Classification of defects, the N_{TB} phase

Perfect line defects are classified by the symmetry elements of the material, according to the matching condition. In the following, we adopt the classic notations of the cholesteric phase [13] for N_{TB}, to which they are well adapted: $\boldsymbol{\chi}$ denotes either the axis of helicity of the director **n** with pitch p (the $\boldsymbol{\chi}$ axis) or the plane perpendicular to it (the $\boldsymbol{\chi}$ plane), $\boldsymbol{\tau}$ denotes a direction normal to the local director in the $\boldsymbol{\chi}$ plane, $\boldsymbol{\lambda} = \boldsymbol{\chi} \times \boldsymbol{\tau}$ is along the projection of **n** on the $\boldsymbol{\chi}$ plane.

The symmetry elements of the N_{TB} phase are:

− *quantized translations* multiple of the pitch p, along the $\boldsymbol{\chi}$ axis

− *binary axes* in $\boldsymbol{\chi}$ planes, normal to the director **n**, i.e., a π rotation along the $\boldsymbol{\tau}$ axis,

− *continuous translations* in the $\boldsymbol{\chi}$ planes, denoted $d\mathbf{u}$,

− *continuous helical rotations* along the $\boldsymbol{\chi}$ axis, i.e., the product of a rotation $d\omega\boldsymbol{\chi}$ and a translation $(p/2\pi)d\omega\boldsymbol{\chi}$.

The corresponding line defects are, in the same order:

− *quantized dislocations* of Burgers vector np, $n \in \mathbb{Z}$,

− *quantized disclinations* of Frank vector $(\pi + 2m\pi)\boldsymbol{\tau}$, $m \in \mathbb{Z}$,

− *continuous dislocations*, Burgers vectors $d\mathbf{u}$,

− *continuous dispirations*, Frank vector $d\mathbf{f} = d\omega\boldsymbol{\chi}$ and Burgers vector $d\mathbf{b} = (p/2\pi)d\omega\boldsymbol{\chi}$.

The above notations are the same as those classically used for the N* phase. The only difference is that in N* **n** is in the $\boldsymbol{\chi}$ plane, along a $\boldsymbol{\lambda}$ direction. Thus, there is N* another set of *binary axes* in the $\boldsymbol{\chi}$ planes, along the $\boldsymbol{\lambda}$ axis. The classification of line defects in a N* phase contains the same defects as in a N_{TB} phase plus a set of *quantized disclinations* of Frank vector $(\pi + 2m\pi)\boldsymbol{\lambda}$, $m \in \mathbb{Z}$.

Notice that the Volterra classification, here and in other phases, is independent of the values of the elastic constants. However, the defect (meta)stability, and the presence of textures involving long distance interactions between defects, are dependent on those constants; it is thereby no surprise that the defects and textures observed in N_{TB} are vastly different from those in a N* phase, although the symmetries are much similar. The elastic constants of the N_{TB} phase are indeed anomalous (in particular, a negative K_{33} constant). How these unusual elastic constants affect the existence and (meta)stability of defects, this important question goes well beyond the scope of this paper.

D. Examples of relaxation mechanisms

We may clarify the relaxation mechanisms in a N_{TB} phase with two examples:

(1) Let $d\mathbf{u}$ be the infinitesimal Burgers vector of a dislocation attached to a disclination of Frank vector along $\boldsymbol{\tau}$, such that [Eq. (1)]

$$d\mathbf{u} = -2\boldsymbol{\tau} \times \mathbf{ds},$$

where $d\mathbf{s}$ is a line element of the disclination (in this equation, the factor 2 stands for the Frank vector modulus $2\sin\Omega/2$, $\Omega = \pi$.) By implication the relevant $d\mathbf{u}$'s have to be taken in a plane perpendicular to $\boldsymbol{\tau}$, thereby along the $\boldsymbol{\lambda}$ direction. Thus, $d\mathbf{s}$ is in a plane perpendicular to $\boldsymbol{\lambda}$. Consequently, the disclination relaxes in such a plane; the tangent **t** to the disclination line is locally normal to a $\boldsymbol{\tau}$ direction.

(2) Consider a wedge loop $k = 1/2$, $\mathbf{f} = 2\boldsymbol{\tau}$, all along the loop. According to Eq. (1) there are attached continuous disclinations with Frank vectors along the (radial) $\boldsymbol{\chi}$ direction, without attached continuous disclinations. These disclinations constitute a part of possible continuous dispirations, but the dislocation part is lacking; the continuous defects attached to the loop are imperfect. In fact, wedge loops in a N_{TB} phase are unstable. See later.

III. DEFECTS ATTACHED TO FOCAL CONIC DOMAINS AND DOUBLE HELICES

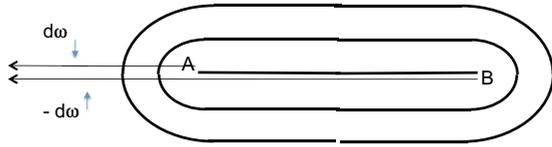Let us now analyze theoretically the defects attached to FCDs and DHs.

FIG. 5. Cut through two $k = 1/2$ wedge disclination lines A and B. The attached infinitesimal disclinations are restricted to the ribbon between A and B, which ribbon can be made to vanish, AB = 0, yielding a $k = 1$ wedge line without attached defects.

A. Toric focal conic domains

As just stated a wedge loop $k = 1/2$ carries a set of imperfect attached defects. The singular circle of a TFCD is such a wedge loop. It is a simple calculation to get

$$\boldsymbol{\tau} = [-\sin\phi, \cos\phi], \qquad \frac{d\boldsymbol{\tau}}{ds} = -\frac{1}{\rho}[\cos\phi, \sin\phi],$$

ρ the circle radius. Hence, $|d\boldsymbol{\tau}/ds|$, a measure of the density of attached disclinations:

$$\left|\frac{d\boldsymbol{\tau}}{ds}\right| = \frac{1}{\rho}.$$

The instability of TFCDs in the N_{TB} phase has to be searched in these imperfect disclination densities, not only because of their presence, but also because in a TFCD the disclinations attached to the circle cannot terminate on the axis, which does not accept attached defects as shown immediately below. Because of this impossibility the area of the stacking fault is not restricted; the attached defects spread with no preferred endings.

The other TFCD singularity is a straight $k = 1$ wedge line whose Frank vector is along $\boldsymbol{\chi}$. This is possible since any axis in space is a 2π rotation axis. There are no attached defects to this $k = 1$ line, even if one may consider that there are attached defects to each half-line of strength $k = 1/2$. The defect densities emanating from each half-line, if oriented in the same direction, are of opposite strength; their sum vanishes outside the ribbon bordered by the two $k = 1/2$ disclinations (Fig. 5).

B. Focal conic domains, $0 < e < 1$

The situation is partly similar; the disclination along the hyperbola is a $k = 1$ wedge line, with $\boldsymbol{\chi}$ axis all along. For the same reason as above it carries no attached defects. The ellipse singularity is more complex than the circle singularity in a TFCD; it is a mixed wedge-twist $k = 1/2$ disclination whose $\boldsymbol{\tau}$ direction appears as the rotation axis when $\boldsymbol{\tau}$ is in the plane of the ellipse (Fig. 6); but $\boldsymbol{\tau}$ rotates helically about the normal to the quasilayers.

In a coarse-grained version of the N_{TB} phase, in which the helical geometry of the director **n** is replaced by the normal to the quasilayers (the optical axis), the symmetry that has to be taken into account is that of the SmA (or the SmA*) [15], and this is indeed what happens empirically for most of the FCDs present in a sample: the defects attached to the ellipse are quantized dislocations (in Ref. [13], p. 110, the ellipse is discussed as a $k = 1/2$ disclination.) To each layer of thickness p traversing the FCD (see Fig. 6) is attached
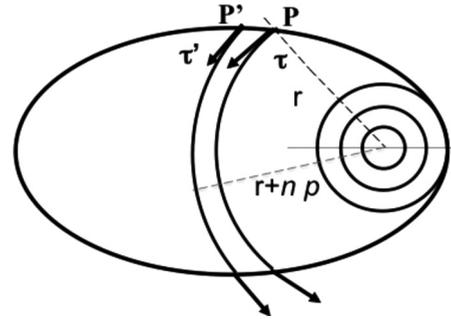

FIG. 6. Along the ellipse of a FCD. Intersections of two cyclides at a distance multiple of p. It is assumed that there is a $\boldsymbol{\tau}$ direction along these intersections; $\boldsymbol{\tau}$ rotates helically about the normal $\boldsymbol{\chi}$ to these cyclides.

a dislocation of Burgers vector $2p$ outside the FCD (not represented in Fig. 6), and an infinitesimal disclination of Frank vector along $\boldsymbol{\tau}' - \boldsymbol{\tau}$ normal to the layer.

The quantized dislocations attached to ellipses in a SmA sample generally cover surface areas between neighboring ellipses and connect them [16]. The same situation occurs in the N_{TB} phase. These quantized dislocations are singularities of the order parameter, whereas the order parameter is continuous inside the ellipses, which results in striking differences in the appearance of the inside and outside regions of an ellipse, with a net discontinuity at the ellipse itself; see Fig. 7.

If the coarse-grained model is not physically achieved, the imperfections are at a nanoscopic scale smaller than p. A distribution of continuous defects attached to the ellipses in place of the quantized dislocations (a fact not possible in the SmA, possible in the N_{TB}), does not carry singularities of the order parameter, other than those of the ellipse itself. Thus, one would expect continuous variations of the observed
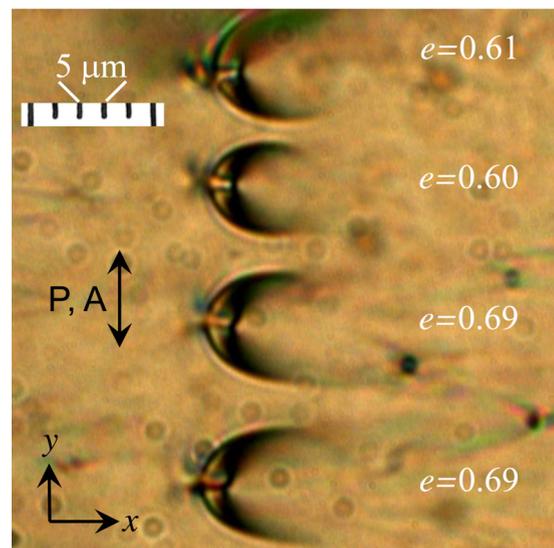

FIG. 7. Quasiparallel FCDs in a 20-μm-thick layer of CB7CB in a planar cell at 0.6°C below the setting point and subjected to a 30 V, 1 kHz field. The FCD ellipses are connected by a set of attached quantized dislocations approximately parallel to the minor axes. P and A denote polarizer and analyzer.

aspect from one side of the ellipse to the other. This is observed for eccentricities close to 1, where the notion of PFCD comes under consideration; see Fig. 2(a) commented hereunder. But in no case can the ellipse arcs be relaxed by continuous dispirations. We discuss later the specific nature of disclination lines that are relaxed by (perfect) continuous dispirations; they are very special, and certainly not conics.

One cannot exclude the possibility that along an ellipse some arcs are relaxed by quantized dislocations, other by continuous defects. Various boundary conditions, or thermal fluctuations, can be at the origin of the choice, which is made possible in a N_{TB} because, structurally, the quantized dislocation picture is coexistent with a continuous defect picture at a smaller scale.

C. Parabolic focal conic domains

PFCDs are very peculiar, compared to the other focal conic domains with $e \neq 1$. If one thinks of a PFCD as the geometrical limit of a FCD when $e \rightarrow 1$, the limit of the ellipse is a parabola carrying a $k = 1/2$ disclination, the limit of the hyperbola a parabola carrying a $k = 1$ disclination. Suppose that the ellipse is equipped with attached quantized dislocations whose total Burgers vector is $4c$ [13], i.e., $4c/2p$ dislocations, $2p$ being the supposed Burgers vector of each one, see above; thus, $2c/2pa = e/p$ dislocations per unit length measured along the major axis. This quantity makes sense even when $e = c/a = 1$, a and c infinite, and the conic is a parabola. This is the largest density of quantized dislocations possibly attached to a conic, hence the largest tilt boundary energy density.

In fact this "asymmetric" picture of a PFCD is valid for any value of e infinitesimally close to 1, but not for $e = 1$. The transition is discontinuous. At $e = 1$, both parabolas carry $k = 1$ disclinations: the axis of any cone with apex **M** on one of the parabolas P_1, whose generatrices lie on the cofocal parabola P_2, is along the tangent t_M to P_1; this cone is of revolution, t_M is an axis of 2π rotation symmetry along which the local Frank vector aligns—not along τ as in the FCD ellipse case. As with $k = 1$ lines in TFCDs and FCDs, there are no defects attached to these parabolas. This is certainly an element of topological and energetical stability of PFCDs, compared to the other types of FCD. A PFCD domain is susceptible to occupy all space. The transition from a FCD to a PFCD has to be discontinuous, physically. It is indeed observed that the nucleation of PFCDs happens spontaneously under stress, but neither from precursory FCDs, nor directly from TFCDs, that are "destroyed" before transforming into PFCDs [10].

D. Double helices

DHs nucleate at the $N \rightarrow$ SmA transition in twist cells, where they proceed from the deformation of twist disclinations into single helices (SHs). The same transformation has been observed at the $N \rightarrow N_{TB}$ transition; see Fig. 3(a). They also evolve from strings of drifting unstable TFCDs; see Figs. 3(b)–3(d).

DHs consist of two helical $k = 1/2$ wedge disclinations with the same axis and the same pitch, shifted one with

respect to the other by half a pitch $P/2$, more or less distorted compared to circular helices. Let ρ be the radius of these helices; this assembly forms a screw dislocation of Burgers vector $b = 2\pi\rho$ [17], i.e., a giant Burgers vector, visible by light microscopy; b is also the pitch P of the helices, $b = P = np$ in a N_{TB} phase. The same geometry has been observed in the B7 banana phase, but in that case with no distortions at all at the scale of light microscopy observations [17,18]. The two helices, being of a wedge type, do not carry attached dislocations, only attached disclinations with Frank vectors along χ directions, thus imperfect attached dispirations.

The equation of a circular helix of radius ρ, pitch $P = b$, can be written

$$x = \rho \cos\phi, \quad y = \rho \sin\phi, \quad z = \frac{b}{2\pi}\phi.$$

The tangent, which is along the τ direction can be written

$$\tau = \left[\rho^2 + \left(\frac{b}{2\pi}\right)^2\right]^{-1/2}\left[-\rho\sin\phi, \; \rho\cos\phi, \; \frac{b}{2\pi}\right].$$

Because of the relation $2\pi\rho = b$, we eventually get

$$\tau = 2^{-1/2}[-\sin\phi, \cos\phi, 1],$$

$$d\tau = 2^{-1/2}[-\cos\phi, -\sin\phi, 0]d\phi.$$

$d\tau$ is along the Frank vector of an attached disclination and along the χ axis; its density measured along the helix is $|d\tau/ds| = \pi/b = 1/(2\rho)$; along the $\hat{z}$ axis it is

$$\left|\frac{d\tau}{dz}\right| = 2^{1/2}\frac{\pi}{b} = 2^{-1/2}\frac{1}{\rho}. \tag{2}$$

The horizontal line segments with Frank vectors $2d\tau$, which rotate helically about $\hat{z}$ with pitch b, form an helicoidal *stacking fault* of width $2\rho = b/\pi$ between the two helical disclinations, thus limited in size. There are no other defects attached to the DH, except possibly those related to the differences with a geometry of perfect circular helices. Apart from the stacking fault contribution to the energy, finite per unit length of DH, one can infer from the dislocation nature of the whole assembly that it is stable due to this very character.

IV. LIGHT MICROSCOPY OBSERVATIONS

Let us apply these considerations to some observed conics. Figure 8 represents a solitary conic, most probably in the midplane of the sample, whose outside interactions are limited to the boundaries. A parabolic polynomial fit yields a coefficient
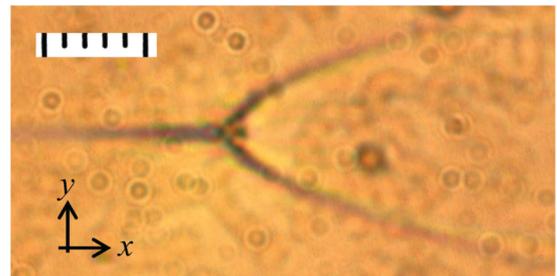

FIG. 8. Solitary PFCD in a 20-μm-thick N_{TB} layer of CB7CB in a planar cell. Scale: 2 μm each small div. Polarizer along x.

TABLE I. Fits of the conics in Fig. 2(a) to ellipses (the two first columns) and parabolas (the last column). R^2 is the coefficient of determination.

	Ellipse R^2	$e(\pm 0.005)$	Parabola R^2
1	1	1	0.9917
2	1	1	0.9987
3	0.9999	0.964	0.7490
4	0.9999	0.965	0.9250
5	0.9999	0.962	0.9501
6	0.9998	0.967	0.9590
7	1	1	0.9972
8	0.9999	0.951	0.9359

of determination $R^2 = 0.9980$, whereas an elliptic fit yields an eccentricity $e = 1$, equal to the eccentricity of a parabola, with $R^2 = 1$! The same type of fitting performed on the conics of Fig. 2(a) (see Fig. 9 of the Appendix for the fitting procedure) yields similar results for the conics numbered 1, 2, and 7 ($R^2 = 1$, $e = 1$ for the elliptic fits, equally large values of R^2 for the parabolic fits.) The conics 3–6 and 8 yield elliptic fits with R^2 and e both ≈ 1, slightly smaller, whereas the parabolic fits yield definitely smaller values of R^2 (typically 0.95 or less) [19]; see Table I and Fig. 9.

A remarkable fact is that the aspect of the FCDs is continuous from one side of those conics to the other, in complete opposition with what is expected for FCDs in a SmA phase. Therefore, the deformation of the material is continuous and the singularity is restricted to the conic. We advance two possibilities:

1. Continuous attached defects

In continuity with the discussion above, the only attached defects would be infinitesimal, thus the deformations continuous except on the conics. Except for those that are PFCDs ($e = 1$), this requires that the conic be a $k = 1/2$ disclination line and the eccentricity e, according to the discussion above, be strictly <1. Since the density of quantized dislocations increases with e, one might then imagine a threshold value of e above which a continuous model is favored (in Fig. 7, e is small),

2. Stacking fault ribbons

Conic defects in layered liquid crystals are seldom "perfect"; they might suffer deformations, which have already been observed, in at least two cases: parabolas in Ref. [9], ellipses in Ref. [20]—in that latter case, the departures from perfect ellipses have been discussed in terms of attached dislocations, quantized or continuous. Whereas ellipses are of $k = 1/2$ disclinations, parabolas are $k = 1$ disclinations that do not accept attached defects. But precisely according to Fig. 5 the $k = 1$ disclination can be split into two close $k = 1/2$ disclinations separated by a stacking fault ribbon made of defects that may deform the conics.

We could in the perspective of stacking faults consider that conics 1, 2, and 7 of Fig. 2(a) and the solitary conic of Fig. 8 are slightly deformed PFCDs, with the parabolic lines

split into two parallel lines. However, conics 3–6, which have seemingly the same eccentricity $e \approx 0.96$, form a fragment of grain boundary of angle $\angle\theta = 2\arcsin e \approx 147°$; obviously they are not connected by attached quantized dislocations, by reason of a continuous appearance. They are most probably connected by continuous defects.

V. ATTACHED DISPIRATIONS AND SPIN DISCLINATIONS

There remains the question of disclination lines carrying attached dispirations of the type $d\omega\boldsymbol{\chi}$ (Frank vector) and $\frac{p}{2\pi}d\omega\boldsymbol{\chi}$ (Burgers vector.) According to Eq. (1), one can write

$$d\mathbf{f} = d\omega\boldsymbol{\chi}, \quad -\mathbf{f} \times \mathbf{t}\,ds = \frac{p}{2\pi}d\omega\boldsymbol{\chi}. \qquad (3)$$

The elimination of $d\omega\boldsymbol{\chi}$ between these equations yields

$$\frac{d\mathbf{f}}{ds} = -\frac{2\pi}{p}\mathbf{f} \times \mathbf{t}. \qquad (4)$$

Let us take $\mathbf{f} = 2\sin(\Omega/2)\boldsymbol{\tau} = 2\boldsymbol{\tau}$ for $\Omega = \pi$, then

$$\frac{d\boldsymbol{\tau}}{ds} = \frac{2\pi}{p}\mathbf{t} \times \boldsymbol{\tau}. \qquad (5)$$

The rotation rate of the Frank vector is $2\pi/p\,\mathbf{t}$, of a constant modulus all along the line. This vector, according to Eq. (3), is along the $\boldsymbol{\lambda}$ direction. Thus, $\mathbf{t}$, $\boldsymbol{\chi}$, $\boldsymbol{\tau}$ form a orthonormal frame; $\mathbf{t}$ is along the local $\boldsymbol{\lambda}$ axis. The disclination is of a pure twist character. The rate of rotation of $\boldsymbol{\chi}$, which is in the plane normal to $\mathbf{t}$, contains two contributions, a rotation about $\mathbf{t}$ with the same rate as $\boldsymbol{\tau}$ and a rotation about $\boldsymbol{\tau}$ with a rate denoted $-1/\rho$, ρ unknown. Thus, $d\boldsymbol{\chi}/ds = (2\pi/p)\boldsymbol{\tau} - (1/\rho)\mathbf{t}$. Also, $d\mathbf{t}/ds = d(\boldsymbol{\chi} \times \boldsymbol{\tau})/ds$, one eventually gets

$$\frac{d\mathbf{t}}{ds} = \frac{1}{\rho}\boldsymbol{\chi},$$
$$\frac{d\boldsymbol{\chi}}{ds} = \frac{2\pi}{p}\boldsymbol{\tau} - \frac{1}{\rho}\mathbf{t},$$
$$\frac{d\boldsymbol{\tau}}{ds} = -\frac{2\pi}{p}\boldsymbol{\chi}, \qquad (6)$$

which are the Frenet formulas for a frame where $\boldsymbol{\chi}$ is the principal normal, $\boldsymbol{\tau}$ the binormal, $\boldsymbol{\lambda} = \mathbf{t}$ the tangent to the line. The torsion of the disclination line is the constant $2\pi/p$; ρ is its radius of curvature. Results of a similar nature were stated in Ref. [13] for cholesterics [21]. Disclinations whose relaxation is due all along their length to continuous dispirations are curves of constant torsion $2\pi/p$; $\boldsymbol{\tau}$ rotates about the line (about $\boldsymbol{\lambda}$) with pitch p, which is small in a N_{TB} phase. Call such a defect a *spin disclination*.

Kœnigs [22] has shown that open curves of constant torsion $2\pi/p$ are periodic along their length. Circular helices are of that type. Let R be the radius of the helix, P its pitch, the torsion $2\pi/p$ and the curvature $1/\rho$ of such an helix can be written

$$\frac{1}{\rho} = \frac{R}{R^2 + P^2/4\pi^2}, \qquad (7a)$$

$$\frac{2\pi}{p} = \frac{P/2\pi}{R^2 + P^2/4\pi^2}. \qquad (7b)$$

These equations are of the second degree in R and P. Taking the first one as an equation with unknown R, a real R requires $\pi\rho > P$; and the second one as an equation with unknown P, a real P requires $4\pi R < p$. Thus, since p is very small, the helix has a microscopic radius and is close to a straight line. Assume then that $R = 0$, which yields $\rho = \infty$, $p = P$. This much twisted disclination is probably of a high energy, but one has a comparable twist of τ and λ along the χ axis in a perfect N_{TB} phase. We haven't observed any defect of the sort. Its search in a N^* phase, where the pitch is large, could be rewarding.

Geometers have actively investigated closed curves of constant torsion, in particular spherical curves; see Ref. [23]. One may wonder whether the small grainy defects observed in the first steps of the instability process of a TFCD (Fig. 1) [10] could not be of this type.

VI. CONCLUSION

To conclude, we have shown that the mere geometrical consideration of defects attached to disclinations, in the framework of the extended Volterra process theory, casts some light on the stability characteristics of the FCDs observed in the N_{TB} phase: the attached continuous defects are imperfect in the sense that they do not carry N_{TB} symmetries. Also, this theory predicts two types of molecular configurations surrounding FCD ellipses, whether their attached defects are continuous or quantized. Both types have been observed, the first one belonging to ellipses of a large eccentricity, close to $e = 1$. Finally, disclinations with (perfect) attached continuous dispirations are special line defects, with a constant torsion. They have not been observed yet. A deeper understanding of the various unusual aspects of defects and textures would require an investigation of the associated energies.

ACKNOWLEDGMENTS

APPENDIX: CURVE FITTINGS

Curve fitting for the conic in the inset. Coordinates (x, y) of various points (indicated by squares) lying on the white
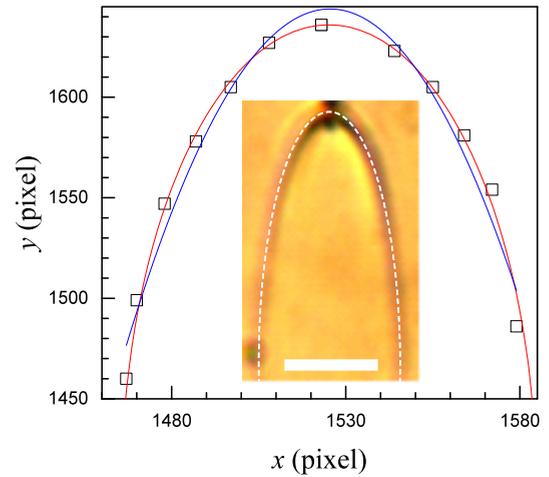
Ellipse	$f = [(x - x_c)/a]^2 + [(y - y_c)/b]^2$	
Reduced Chi-S	1.31233	
Adj. R-Square	0.9999	
	Value	Std. Error
x_c	1887.5	0.38
y_c	1580.7	12.30
a	66	1.07
b	214	12.67
$e = \sqrt{[1-(a/b)^2]}$	0.9514	0.0045

Parabola	$y = A x^2 + B x + C$	
Residual sum of squares	2614	
Adj. R-Square	0.9359	
	Value	Std. Error
C	-148526	11936
A	159.4	12.6
B	-0.0422	0.0033

FIG. 9. Curve fittings, see text.

median dashed line of the conic were chosen for the purpose of fitting. The parameters of fitting as given by the Origin 9.1 software are tabulated below the plot in which blue and red lines are for parabola and ellipse, respectively; $0.11\,\mu$m/pixel, scale bar $= 10\,\mu$m. A $50\times$ objective of NA 0.55 was used in textural studies. Corresponding distance resolution is $\sim 0.5\,\mu$m or ~ 5 pix; thus, a, b, and e are to be considered as 66 ± 3 pix, 214 ± 3 pix, and 0.952 ± 0.005, respectively.

[1] R. B. Meyer, Phys. Rev. Lett. **22**, 918 (1969).

[2] I. Dozov, Europhys. Lett. **56**, 247 (2001).

[3] C. Meyer, G. R. Luckhurst, and I. Dozov, Phys. Rev. Lett. **111**, 067801 (2013).

[4] S. A. Pardaev, S. M. Shamid, M. G. Tamba, C. Welch, G. H. Mehl, J. T. Gleeson, D. W. Allender, J. V. Selinger, B. Ellman, A. Jákli, and S. Sprunt, Soft Matter **12**, 4472 (2016).

[5] V. P. Panov, M. Nagaraj, J. K. Vij, Y. P. Panarin, A. Kohlmeier, M. G. Tamba, R. A. Lewis, and G. H. Mehl, Phys. Rev. Lett. **105**, 167801 (2010).

[6] M. Cestari, S. Diez-Berart, D. A. Dunmur, A. Ferrarini, M. R. de la Fuente, D. J. B. Jackson, D. O. Lopez, G. R. Luckhurst, M. A. Perez-Jubindo, R. M. Richardson, J. Salud, B. A. Timimi, and H. Zimmermann, Phys. Rev. E **84**, 031704 (2011).

[7] V. Borschch, Y. Kim, J. Xiang, A. Jákli, V. P. Panov, J. K. Vij, C. T. Imrie, M. G. Tamba, G. H. Mehl, and O. D. Lavrentovich, Nat. Commun. **4**, 2635 (2013).

[8] V. P. Panov, M. C. M. Varney, I. I. Smalyukh, J. K. Vij, M. G. Tamba, and G. H. Mehl, Mol. Cryst. Liq. Cryst. **611**, 180 (2015).

[9] C. S. Rosenblatt, S. Pindak, N. A. Clark, and R. B. Meyer, Journal de physique **38**, 1105 (1977).

[10] K. S. Krishnamurthy, M. B. Kanakala, C. V. Yelamaggad, and M. Kleman, Soft Matter **14**, 5393 (2018).

[11] C. E. Williams, Philos. Mag. **32**, 313 (1975).

[12] S. Parthasarathi, D. S. S. Rao, N. B. Palakurthy, C. V. Yelamaggad, and S. K. Prasad, J. Phys. Chem. B **120**, 5056 (2016).

[13] M. Kleman and J. Friedel, Rev. Mod. Phys. **80**, 61 (2008).

[14] M. Kleman and J. Friedel, Journal de physique **30**, C4-43 (1969).

[15] I. Dozov and C. Meyer, Liq. Cryst. **44**, 4 (2017).

[16] M. Kleman and O. D. Lavrentovich, Eur. Phys. J. E **2**, 47 (2000).

[17] M. Kleman, O. D. Lavrentovich, and Y. A. Nastishin, *Dislocations and Disclinations in Mesomorphic Phases*, edited by F. R. N. Nabarro and J. P. Hirth (Elsevier, Amsterdam, The Netherlands, 2004), Chap. 66, p. 147.

[18] M.-F. Achard, M. Kleman, Y. A. Nastishin, and H. T. Nguyen, Eur. Phys. J. E **16**, 37 (2005).

[19] See the Appendix for a discussion of the accuracy of the fits.

[20] Y. A. Nastishin, C. Meyer, and M. Kleman, Liq. Cryst. **35**, 609 (2008).

[21] The demonstration given in Ref. [13] is incomplete—it assumes implicitly that the trihedron λ, χ, τ is a Frenet frame—and includes an error of sign.

[22] G. Koenigs, Ann. Fac. Sci. Toulouse 1re série **1**, E1 (1887).

[23] A. Calini and T. Ivey, J. Knot Theory Ramificat. **7**, 719 (1998).